

Noname manuscript No.
 (will be inserted by the editor)

The Kinematics and Dynamics Theories of a Total Lagrangian Finite Element Analysis Framework for Finite Deformation Multibody Dynamics

Zhenhao Zhou · Ganesh Arivoli · Dan Negrut

Abstract This work presents a Total Lagrangian (TL) finite element formulation for deformable body dynamics. We employ the TL-FEA framework to simulate the time evolution of collections of bodies whose motion is constrained by kinematic constraints and which mutually interact through contact and friction. These bodies experience large displacements, large deformations, and large rotations. A systematic approach is proposed for classifying and posing kinematic constraints acting between the bodies present in the system. We derive the governing equations for ANCF beam, ANCF shell, and tetrahedral elements, and present hyperelastic material models including St. Venant–Kirchhoff and Mooney–Rivlin formulations with their corresponding internal force contributions and consistent tangent stiffness matrices. A finite-strain Kelvin–Voigt viscous damping model is incorporated in the TL-FEA formulation for numerical stability.

Keywords Total Lagrangian · finite element analysis · multibody dynamics · hyperelasticity · augmented Lagrangian

Mathematics Subject Classification (2020) 74B20 · 74S05 · 74H55

1 Formulation for Deformable Elements

In handling the time evolution of deformable bodies that experience large displacements, large deformations, and large rotations, one can use the Total

Z. Zhou
 University of Wisconsin–Madison
 E-mail: zzhou292@wisc.edu

G. Arivoli
 University of Wisconsin–Madison
 E-mail: arivoli@wisc.edu

D. Negrut
 University of Wisconsin–Madison
 E-mail: negrut@wisc.edu

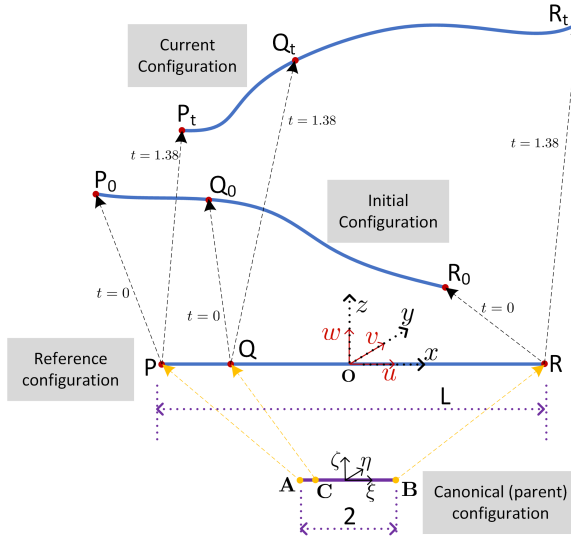


Fig. 1 Key element configurations.

Lagrangian (TL) or the Updated Lagrangian (UL) approaches. Here, we embrace the former, a methodology that is approximately five decades old [22]. Our goal is to establish a general TL-FEA framework that can naturally handle complex multibody systems, i.e., one can have multiple bodies, their motion can be constrained by kinematic constraints, and they can mutually interact through contact and friction.

1.1 Key Element Configurations

The elements discussed here are volumetric elements. The nodal unknowns can be either positions only, or, just as in ANCF [17], they can be a combination of positions and position gradients.

The reference configuration of an element is that in which the element experiences no strain and no stress. Typically, this is the undeformed configuration of the element, as produced by a mesher, e.g., **Gmsh** [6] or **TetGen** [18]. Associated with this reference configuration there is a reference frame $Ouvw$, whose position and orientation are fixed in space. A point P in the reference configuration of coordinates (u, v, w) is mapped at time t into a different point, which has coordinates $\mathbf{r}(u, v, w; t) = [x(u, v, w; t), y(u, v, w; t), z(u, v, w; t)]^T$ in a global reference frame $Oxyz$. The deformation map φ is the mapping that takes a point in the reference configuration to a point in the current configuration. The deformation map is a function of the time t and the material coordinates \mathbf{u} , i.e., $\varphi = \varphi(\mathbf{u}; t)$, where $\mathbf{u} = [u, v, w]^T$. The initial configuration is the configuration of the element at time $t = 0$. Finally, the parent (or canonical) configuration is used to carry out the numerical integration over

the volume of the element. The elements can be iso-parametric, or, for simple cases, the mapping between the parent and the reference configuration can be an affine transformation.

1.2 Interpolation Across the Element

Since the deformation map cannot be produced analytically, the FEA method uses an interpolation approach to approximate a field variable using the nodal values. Here, the “field variable” of interest is the position \mathbf{r} of a point that in the reference configuration is at coordinates $\mathbf{u} = [u, v, w]^T$. The interpolation is carried out using the matrix of nodal unknowns $\mathbf{N}(t) = [\mathbf{e}_1(t), \dots, \mathbf{e}_{n_u}(t)] \in \mathbb{R}^{3 \times n_u}$ and the array of shape functions $\mathbf{s}(u, v, w) = [s_1(u, v, w), \dots, s_{n_u}(u, v, w)]^T \in \mathbb{R}^{n_u}$,

$$\begin{aligned}\mathbf{r}(u, v, w; t) &= \mathbf{N}(t) \mathbf{s}(u, v, w) \\ &= \sum_{i=1}^{n_u} \mathbf{e}_i(t) s_i(u, v, w) .\end{aligned}$$

This leads to $\dot{\mathbf{r}}(u, v, w; t) = \dot{\mathbf{N}}(t) \mathbf{s}(u, v, w)$, $\ddot{\mathbf{r}}(u, v, w; t) = \ddot{\mathbf{N}}(t) \mathbf{s}(u, v, w)$, and the deformation gradient

$$\begin{aligned}\mathbf{F} &= \frac{\partial \mathbf{r}}{\partial \mathbf{u}} = \mathbf{N}(t) \mathbf{H}(u, v, w) \\ &= \sum_{i=1}^{n_u} \mathbf{e}_i(t) \mathbf{h}_i^\top(u, v, w) , \\ \mathbf{h}_i^\top(u, v, w) &\coloneqq \frac{\partial s_i(u, v, w)}{\partial \mathbf{u}} , \\ \mathbf{H}(u, v, w) &\coloneqq \frac{\partial \mathbf{s}(u, v, w)}{\partial \mathbf{u}} .\end{aligned}\tag{1}$$

1.3 Sample Element Types

1.3.1 3243 ANCF Beam Element

The most basic element considered in the comparison is the original 2-node ANCF beam element 3243, which is fully parameterized, as referenced in [5]. As illustrated in Fig. 2.1, each node is described by 12 coordinates, including a position vector \mathbf{r}_i and its gradients with respect to the local coordinates u , v , and w , denoted as $\frac{\partial \mathbf{r}_i}{\partial u}$, $\frac{\partial \mathbf{r}_i}{\partial v}$, and $\frac{\partial \mathbf{r}_i}{\partial w}$. This full set of coordinates per node defines the “fully parameterized” terminology. With two such nodes, the element possesses 24 degrees of freedom when unconstrained. The visualization of this element can be seen in Figure 2.

The vector of basis function for 3243 beam element is:

$$\mathbf{b}^T(u, v, w) = [1, u, v, w, uv, uw, u^2, u^3]$$

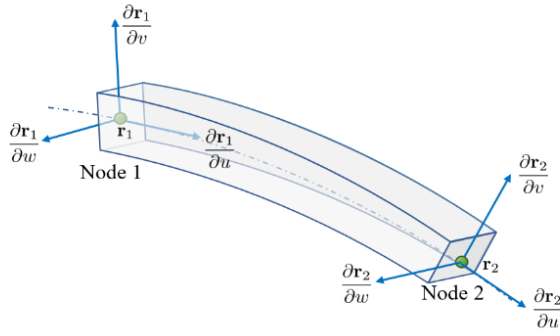


Fig. 2 Visualization of a fully-parameterized 2-node ANCF beam element 3243.

The constant matrix $\mathbf{B}_{12} \in \mathbb{R}^{8 \times 8}$ can be defined as:

$$\mathbf{B}_{12} \equiv [\mathbf{b}(P_1), \mathbf{b}_{,u}(P_1), \mathbf{b}_{,v}(P_1), \mathbf{b}_{,w}(P_1), \mathbf{b}(P_2), \mathbf{b}_{,u}(P_2), \mathbf{b}_{,v}(P_2), \mathbf{b}_{,w}(P_2)]^T,$$

Therefore, the time-dependent global nodal coordinates, as well as the gradients components, x_{12} , y_{12} , and z_{12} ,

$$\begin{aligned} \mathbf{x}_{12}^T &\equiv [x_1, x_{1,u}, x_{1,v}, x_{1,w}, x_2, x_{2,u}, x_{2,v}, x_{2,w}], \\ \mathbf{y}_{12}^T &\equiv [y_1, y_{1,u}, y_{1,v}, y_{1,w}, y_2, y_{2,u}, y_{2,v}, y_{2,w}], \\ \mathbf{z}_{12}^T &\equiv [z_1, z_{1,u}, z_{1,v}, z_{1,w}, z_2, z_{2,u}, z_{2,v}, z_{2,w}]. \end{aligned}$$

as well as the unknown coefficients α , β , and γ :

$$\begin{aligned} \mathbf{B}_{12}^T \cdot \boldsymbol{\alpha} &= \mathbf{x}_{12} & \Rightarrow \quad \boldsymbol{\alpha} &= \mathbf{B}_{12}^{-T} \cdot \mathbf{x}_{12}, \\ \mathbf{B}_{12}^T \cdot \boldsymbol{\beta} &= \mathbf{y}_{12} & \Rightarrow \quad \boldsymbol{\beta} &= \mathbf{B}_{12}^{-T} \cdot \mathbf{y}_{12}, \\ \mathbf{B}_{12}^T \cdot \boldsymbol{\gamma} &= \mathbf{z}_{12} & \Rightarrow \quad \boldsymbol{\gamma} &= \mathbf{B}_{12}^{-T} \cdot \mathbf{z}_{12}. \end{aligned}$$

which leads to:

$$[\boldsymbol{\alpha} \ \boldsymbol{\beta} \ \boldsymbol{\gamma}] = \mathbf{B}_{12}^{-T} [\mathbf{x}_{12} \ \mathbf{y}_{12} \ \mathbf{z}_{12}].$$

$$\begin{bmatrix} \boldsymbol{\alpha}^T \\ \boldsymbol{\beta}^T \\ \boldsymbol{\gamma}^T \end{bmatrix} = \begin{bmatrix} \mathbf{x}_{12}^T \\ \mathbf{y}_{12}^T \\ \mathbf{z}_{12}^T \end{bmatrix} \mathbf{B}_{12}^{-1},$$

which means that:

$$\mathbf{r}(u, v, w, t) = \begin{bmatrix} \mathbf{x}_{12}^T \\ \mathbf{y}_{12}^T \\ \mathbf{z}_{12}^T \end{bmatrix} \mathbf{B}_{12}^{-1} \cdot \mathbf{b}(u, v, w) = \mathbf{N}(t) \cdot \mathbf{s}(u, v, w),$$

where $\mathbf{N}(t) \in \mathbb{R}^{3 \times 8}$ and $\mathbf{s}(u, v, w) \in \mathbb{R}^{8 \times 1}$ are defined as:

$$\begin{aligned} \mathbf{N}(t) &\equiv \begin{bmatrix} x_1 & x_{1,u} & x_{1,v} & x_{1,w} & x_2 & x_{2,u} & x_{2,v} & x_{2,w} \\ y_1 & y_{1,u} & y_{1,v} & y_{1,w} & y_2 & y_{2,u} & y_{2,v} & y_{2,w} \\ z_1 & z_{1,u} & z_{1,v} & z_{1,w} & z_2 & z_{2,u} & z_{2,v} & z_{2,w} \end{bmatrix} \\ &= [\mathbf{r}_1 \ \mathbf{r}_{1,u} \ \mathbf{r}_{1,v} \ \mathbf{r}_{1,w} \\ &\quad \mathbf{r}_2 \ \mathbf{r}_{2,u} \ \mathbf{r}_{2,v} \ \mathbf{r}_{2,w}] \\ &\equiv [\mathbf{e}_1 \ \mathbf{e}_2 \ \mathbf{e}_3 \ \mathbf{e}_4 \\ &\quad \mathbf{e}_5 \ \mathbf{e}_6 \ \mathbf{e}_7 \ \mathbf{e}_8], \end{aligned} \quad (2a)$$

with $\mathbf{e}_i \in \mathbb{R}^3$, for $1 \leq i \leq 8$, and the shape function is defined as

$$\mathbf{s}(u, v, w) \equiv \mathbf{B}_{12}^{-1} \cdot \mathbf{b}(u, v, w) \in \mathbb{R}^8. \quad (2b)$$

1.3.2 ANCF 3443 Shell Element

The 3443 ANCF shell element is a fully parameterized 4-node element, as shown in Figure 3. Each of the four nodes in this quadrilateral element is defined by a position vector and three corresponding position vector gradients. Altogether, this configuration yields 48 degrees of freedom for a single unconstrained element, which is double that of the fully parameterized 2-node ANCF beam element 3243.

The vector of basis function for 3443 shell element is:

$$\mathbf{b}^T(u, v, w) = [1, u, v, w, uw, vw, uv, u^2, w^2, u^3, w^3, u^2w, w^2u, uvw, u^3w, uw^3]$$

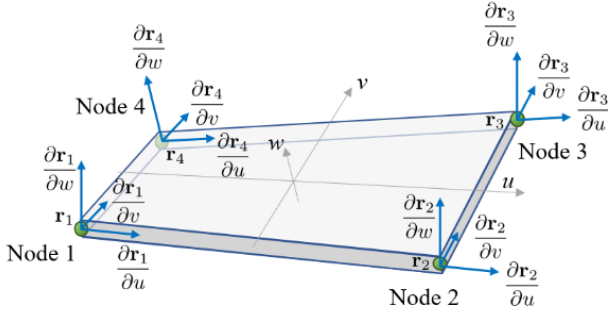


Fig. 3 Visualization of a fully-parameterized 4-node ANCF shell element 3443.

The constant interpolation matrix $\mathbf{B} \in \mathbb{R}^{16 \times 16}$ can be constructed by evaluating the basis functions and their partial derivatives with respect to the material coordinates (u, v, w) at each of the four nodes:

$$\begin{aligned} \mathbf{B}_{1234} &= [\mathbf{b}(P_1), \mathbf{b}_{,u}(P_1), \mathbf{b}_{,v}(P_1), \mathbf{b}_{,w}(P_1), \\ &\quad \dots, \mathbf{b}(P_4), \mathbf{b}_{,u}(P_4), \mathbf{b}_{,v}(P_4), \mathbf{b}_{,w}(P_4)] \end{aligned}$$

The time-dependent global nodal coordinates can be grouped similarly to the beam case, into three vectors containing the x , y , and z components across all nodes and their gradients:

$$\begin{aligned}\mathbf{x}_{1234}^\top &\equiv [x_1, x_{1,u}, x_{1,v}, x_{1,w}, x_2, x_{2,u}, x_{2,v}, x_{2,w}, \\ &\quad x_3, x_{3,u}, x_{3,v}, x_{3,w}, x_4, x_{4,u}, x_{4,v}, x_{4,w}], \\ \mathbf{y}_{1234}^\top &\equiv [y_1, y_{1,u}, y_{1,v}, y_{1,w}, y_2, y_{2,u}, y_{2,v}, y_{2,w}, \\ &\quad y_3, y_{3,u}, y_{3,v}, y_{3,w}, y_4, y_{4,u}, y_{4,v}, y_{4,w}], \\ \mathbf{z}_{1234}^\top &\equiv [z_1, z_{1,u}, z_{1,v}, z_{1,w}, z_2, z_{2,u}, z_{2,v}, z_{2,w}, \\ &\quad z_3, z_{3,u}, z_{3,v}, z_{3,w}, z_4, z_{4,u}, z_{4,v}, z_{4,w}].\end{aligned}$$

As with the 3243 element, the unknown coefficient vectors $\boldsymbol{\alpha}$, $\boldsymbol{\beta}$, and $\boldsymbol{\gamma}$ can be determined using the inverse of the matrix \mathbf{B} :

$$\begin{aligned}\boldsymbol{\alpha} &= \mathbf{B}^{-T} \cdot \mathbf{x}_{1234}, \\ \boldsymbol{\beta} &= \mathbf{B}^{-T} \cdot \mathbf{y}_{1234}, \\ \boldsymbol{\gamma} &= \mathbf{B}^{-T} \cdot \mathbf{z}_{1234}.\end{aligned}$$

Therefore, the position vector field can be expressed as:

$$\mathbf{r}(u, v, w; t) = \begin{bmatrix} \mathbf{x}_{1234}^\top \\ \mathbf{y}_{1234}^\top \\ \mathbf{z}_{1234}^\top \end{bmatrix} \mathbf{B}_{1234}^{-1} \cdot \mathbf{b}(u, v, w) = \mathbf{N}(t) \cdot \mathbf{s}(u, v, w),$$

where $\mathbf{N}(t) \in \mathbb{R}^{3 \times 16}$ and $\mathbf{s}(u, v, w) \in \mathbb{R}^{16 \times 1}$ are defined as:

$$\begin{aligned}\mathbf{N}(t) &\equiv \begin{bmatrix} x_1 & x_{1,u} & x_{1,v} & x_{1,w} & x_2 & x_{2,u} & x_{2,v} & x_{2,w} & x_3 & x_{3,u} & x_{3,v} & x_{3,w} & x_4 & x_{4,u} & x_{4,v} & x_{4,w} \\ y_1 & y_{1,u} & y_{1,v} & y_{1,w} & y_2 & y_{2,u} & y_{2,v} & y_{2,w} & y_3 & y_{3,u} & y_{3,v} & y_{3,w} & y_4 & y_{4,u} & y_{4,v} & y_{4,w} \\ z_1 & z_{1,u} & z_{1,v} & z_{1,w} & z_2 & z_{2,u} & z_{2,v} & z_{2,w} & z_3 & z_{3,u} & z_{3,v} & z_{3,w} & z_4 & z_{4,u} & z_{4,v} & z_{4,w} \end{bmatrix} \\ &= [\mathbf{e}_1 \ \mathbf{e}_2 \ \dots \ \mathbf{e}_{16}], \quad \text{with } \mathbf{e}_i \in \mathbb{R}^3\end{aligned}\tag{3a}$$

$$\mathbf{s}(u, v, w) \equiv \mathbf{B}_{1234}^{-1} \cdot \mathbf{b}(u, v, w) \in \mathbb{R}^{16}.\tag{3b}$$

1.3.3 10-Node Tetrahedron Element

The 10-node tetrahedron (T10), as shown in Figure 4, is a quadratic isoparametric solid element defined on a reference (parent) tetrahedron in the parametric coordinates (ξ, η, ζ) with

$$\xi \geq 0, \quad \eta \geq 0, \quad \zeta \geq 0, \quad \xi + \eta + \zeta \leq 1.\tag{4}$$

It contains four corner nodes at the vertices of the simplex and six nodes located at the midpoints of the edges. The nodal positions in the parent domain can be expressed in barycentric coordinates L_i ($i = 1, \dots, 4$),

$$L_1 = 1 - \xi - \eta - \zeta, \quad L_2 = \xi, \quad L_3 = \eta, \quad L_4 = \zeta,\tag{5}$$

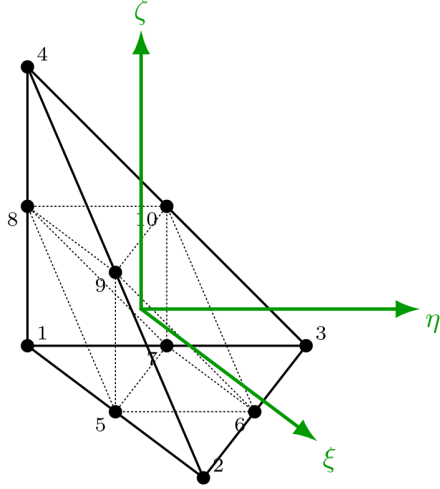


Fig. 4 Visualization of a 10-node tetrahedron (T10) element.

which satisfy $L_i \geq 0$ and $L_1 + L_2 + L_3 + L_4 = 1$. The four vertex nodes correspond to $L_i = 1$ at each corner, and the six mid-edge nodes correspond to $L_i = L_j = 1/2$ on each edge (i, j) .

The T10 element employs the quadratic Lagrange basis on the tetrahedral simplex. In terms of barycentric coordinates, the shape functions for the four corner nodes are

$$\begin{aligned} N_1 &= L_1(2L_1 - 1), \\ N_2 &= L_2(2L_2 - 1), \\ N_3 &= L_3(2L_3 - 1), \\ N_4 &= L_4(2L_4 - 1), \end{aligned} \quad (6)$$

and the six edge-midpoint nodes are

$$\begin{aligned} N_5 &= 4L_1L_2, & N_6 &= 4L_2L_3, & N_7 &= 4L_3L_1, \\ N_8 &= 4L_1L_4, & N_9 &= 4L_2L_4, & N_{10} &= 4L_3L_4. \end{aligned} \quad (7)$$

These functions form a complete basis for all polynomials of total degree ≤ 2 on the tetrahedron (dimension 10) and satisfy the usual isoparametric properties:

$$\sum_{a=1}^{10} N_a(\xi, \eta, \zeta) = 1, \quad N_a(\xi_b, \eta_b, \zeta_b) = \delta_{ab}, \quad (8)$$

which implies C^0 continuity across conforming meshes and Kronecker delta interpolation of nodal degrees of freedom.

Let \mathbf{X}_a and \mathbf{x}_a denote the nodal positions in the reference and current configurations, respectively, and let $\mathbf{d}_a = \mathbf{x}_a - \mathbf{X}_a$ be the displacement of node a .

The isoparametric mappings for the reference position and displacement fields inside the element are

$$\begin{aligned}\mathbf{X}(\xi, \eta, \zeta) &= \sum_{a=1}^{10} N_a(\xi, \eta, \zeta) \mathbf{X}_a, \\ \mathbf{u}(\xi, \eta, \zeta) &= \sum_{a=1}^{10} N_a(\xi, \eta, \zeta) \mathbf{d}_a.\end{aligned}\quad (9)$$

The current position is $\mathbf{x} = \mathbf{X} + \mathbf{u}$, and the deformation gradient in the Total Lagrangian setting is obtained from

$$\mathbf{F}(\xi, \eta, \zeta) = \frac{\partial \mathbf{x}}{\partial \mathbf{X}} = \frac{\partial \mathbf{x}}{\partial(\xi, \eta, \zeta)} \left(\frac{\partial \mathbf{X}}{\partial(\xi, \eta, \zeta)} \right)^{-1}. \quad (10)$$

Both Jacobians are computed from the shape function derivatives $N_{a,\xi}$, $N_{a,\eta}$, $N_{a,\zeta}$, and the nodal coordinates \mathbf{X}_a , so that the standard Total Lagrangian strain measures and element strain-displacement matrix \mathbf{B} follow directly.

Element integrals in the reference configuration are evaluated over the parent tetrahedron using Gaussian quadrature. In this work we employ a five-point rule that is exact for polynomials of total degree up to three, with quadrature points (ξ_q, η_q, ζ_q) and weights W_q chosen such that

$$\int_{\Omega_0^e} (\cdot) \, dV = \int_{\hat{\Omega}} (\cdot) J(\xi, \eta, \zeta) \, d\xi \, d\eta \, d\zeta \approx \sum_{q=1}^5 (\cdot)_q J_q W_q, \quad (11)$$

where $\hat{\Omega}$ is the parent tetrahedron, $J = \det(\partial \mathbf{X} / \partial(\xi, \eta, \zeta))$ is the geometric Jacobian, and $(\cdot)_q$ denotes the integrand evaluated at quadrature point q . The same quadrature rule is used for both mass and internal-force contributions, providing a consistent and robust discretization for the T10 element.

2 Augmented Lagrangian Formulation

Start by assuming the position-level kinematic constraint equations read:

$$c_i(\mathbf{r}_{n+1}, \mathbf{A}_{n+1}, t_{n+1}) = 0, \quad i = 1, 2, \dots, m, \quad (12)$$

and they combine to form the vector of constraints $\mathbf{c}(\mathbf{r}_{n+1}, \mathbf{A}_{n+1}, t_{n+1}) = \mathbf{0}$. For compactness, define $c_i^{n+1} := c_i(\mathbf{r}_{n+1}, \mathbf{A}_{n+1}, t_{n+1})$. ALM starts with the Lagrangian function:

$$\mathcal{L}_\rho(\dot{\mathbf{v}}_{n+1}, \bar{\omega}_{n+1}, \boldsymbol{\lambda}) = \ell(\dot{\mathbf{v}}_{n+1}, \bar{\omega}_{n+1}) + \sum_{i=1}^m \left[\lambda_i c_i^{n+1} + \frac{\rho_i}{2} (c_i^{n+1})^2 \right], \quad (13)$$

where ρ_i are penalty parameters that control the weight of the quadratic penalty term, and λ_i are the Lagrange multipliers, i.e., the dual variables. The constraint functions $c_i(\mathbf{r}_{n+1}, \mathbf{A}_{n+1}, t_{n+1})$ are evaluated at the position level and

depend implicitly on the optimization variables $\dot{\mathbf{v}}_{n+1}$ and $\bar{\boldsymbol{\omega}}_{n+1}$ through the integration scheme used to compute the updated position \mathbf{r}_{n+1} and orientation \mathbf{A}_{n+1} .

The optimization approach, either first-order or second-order, can be used to minimize the cost functions in Eqs. 13 and 14. For the velocity level approach to solving the constrained multibody dynamics problem, see Eq. 14, the constraints are abstracted as

$$\mathbf{c}(\mathbf{x}) = \mathbf{0}, \quad \text{where } \mathbf{x} = \begin{bmatrix} \dot{\mathbf{v}}_{n+1} \\ \bar{\boldsymbol{\omega}}_{n+1} \end{bmatrix}.$$

The Augmented Lagrangian for this problem is

$$\mathcal{L}_{\boldsymbol{\rho}}(\mathbf{x}, \boldsymbol{\lambda}) = \ell(\mathbf{x}) + \sum_{i=1}^m \left[\lambda_i \tilde{\nu}_i(\mathbf{x}) + \frac{\rho_i}{2} \tilde{\nu}_i(\mathbf{x})^2 \right], \quad (14)$$

where $\ell(\mathbf{x})$ is the cost function, λ_i are the Lagrange multipliers, and $\rho_i > 0$ are penalty weights associated with each constraint.

In the proposed framework for solving the Total Lagrangian finite element analysis for multibody dynamics, we derive the equations of motion from the principle of virtual work. The total virtual work is written as:

$$\delta W = \delta W_{\text{inertia}} + \delta W_{\text{applied}} + \delta W_{\text{force-field}} + \delta W_{\text{internal}}, \quad (15)$$

where $\delta W_{\text{inertia}}$, $\delta W_{\text{applied}}$, $\delta W_{\text{force-field}}$, and $\delta W_{\text{internal}}$ denote the virtual works of the inertial terms, applied forces, mass-distributed force fields, and internal forces, respectively. Imposing $\delta W = 0$ and factoring out the virtual generalized displacements yields an expression of the form:

$$\sum_{i=1}^{n_u} \delta \mathbf{q}_i^T \mathbf{g}_i = 0, \quad (16)$$

where $\delta \mathbf{q}_i$ is an arbitrary virtual displacement associated with the i th nodal unknown and \mathbf{g}_i is the corresponding residual contribution. Since $\delta \mathbf{q}_i$ are arbitrary, Eq. (16) implies $\mathbf{g}_i = \mathbf{0}$ for all i , which yields the discrete equations of motion.

In the following sections, we derive the expressions for all contribution terms that make up Eq. (15). The inertial term is derived in Section 3. The mass-distributed force fields are discussed in Section 4, and the internal forces are discussed in Section 5. Finally, the applied forces, which in the majority of problems come from friction and contact and external applied force loads, are discussed in Section 6.

With the update $\mathbf{q}_{n+1} = \mathbf{q}_n + h \mathbf{v}_{n+1}$, the residual can be written as:

$$\begin{aligned} \mathbf{g}(\mathbf{v}, \boldsymbol{\lambda}) = & \frac{1}{h} \mathbf{M}(\mathbf{v} - \mathbf{v}_n) + \mathbf{f}_{\text{int}}(\mathbf{q}_n + h\mathbf{v}, \mathbf{v}) - \mathbf{f}_{\text{ext}} - \mathbf{f}_{\text{ff}} \\ & + h \mathbf{J}(\mathbf{q}_n + h\mathbf{v})^T (\boldsymbol{\lambda} + \rho \mathbf{c}(\mathbf{q}_n + h\mathbf{v})) , \end{aligned} \quad (17)$$

where \mathbf{M} is a preassembled and constant mass matrix of the dynamic system, ρ is the ALM penalty parameter, and $\mathbf{c}(\mathbf{q}) = \mathbf{0}$ denotes bilateral constraints with

Jacobian $\mathbf{J} = \partial \mathbf{c} / \partial \mathbf{q}$. Note that $\mathbf{c}(\mathbf{q}) \in \mathbb{R}^m$ is a constraint-space quantity and is mapped to the generalized space through $\mathbf{J}(\cdot)^T$ in Eq. (17). We evaluate $\mathbf{J}^T(\cdot)$ via a sparse representation of \mathbf{J}^T , and enforce constraints with an augmented-Lagrangian outer loop that alternates an inner solve for \mathbf{v} with multiplier updates until $\|\mathbf{c}\|_2$ meets a prescribed tolerance.

In Eq. (17), $\mathbf{f}_{\text{int}}(\mathbf{q}, \mathbf{v})$ denotes the assembled internal force vector induced by material deformation (including elastic and viscous contributions), while \mathbf{f}_{ext} collects applied loads specified directly as external nodal forces (including point loads and contact/friction forces treated as external). The term \mathbf{f}_{ff} accounts for mass-distributed force fields (body forces) specified per unit mass, such as gravity; although it can be absorbed into \mathbf{f}_{ext} , we keep it separate to emphasize its origin in the force-field virtual work component in Eq. (15).

The residual form in Eq. (17) can be interpreted as the first-order optimality condition of a scalar augmented objective in the velocity unknown. Introduce the step map $\mathbf{q}(\mathbf{v}) := \mathbf{q}_n + h\mathbf{v}$, and assume that the internal force operator admits an incremental potential $\Pi_{\text{int}}(\mathbf{q}, \mathbf{v})$ such that $\nabla_{\mathbf{v}}(\frac{1}{h}\Pi_{\text{int}}(\mathbf{q}(\mathbf{v}), \mathbf{v})) = \mathbf{f}_{\text{int}}(\mathbf{q}(\mathbf{v}), \mathbf{v})$. Then the residual $\mathbf{g}(\mathbf{v}, \boldsymbol{\lambda})$ is obtained by differentiating the discrete augmented Lagrangian cost:

$$\begin{aligned} \Phi_{\rho}(\mathbf{v}, \boldsymbol{\lambda}) &= \frac{1}{2h} (\mathbf{v} - \mathbf{v}_n)^T \mathbf{M} (\mathbf{v} - \mathbf{v}_n) \\ &\quad + \frac{1}{h} \Pi_{\text{int}}(\mathbf{q}_n + h\mathbf{v}, \mathbf{v}) - \mathbf{f}_{\text{ext}}^T \mathbf{v} - \mathbf{f}_{\text{ff}}^T \mathbf{v} \\ &\quad + \boldsymbol{\lambda}^T \mathbf{c}(\mathbf{q}_n + h\mathbf{v}) \\ &\quad + \frac{\rho}{2} \|\mathbf{c}(\mathbf{q}_n + h\mathbf{v})\|_2^2. \end{aligned} \quad (18)$$

Using $\nabla_{\mathbf{v}} \mathbf{c}(\mathbf{q}_n + h\mathbf{v}) = h\mathbf{J}(\mathbf{q}_n + h\mathbf{v})$ and the chain rule, one verifies that $\nabla_{\mathbf{v}} \Phi_{\rho}(\mathbf{v}, \boldsymbol{\lambda}) = \mathbf{g}(\mathbf{v}, \boldsymbol{\lambda})$. Consequently, for fixed multipliers $\boldsymbol{\lambda}$, the inner solve $\mathbf{g}(\mathbf{v}, \boldsymbol{\lambda}) = \mathbf{0}$ is equivalent to enforcing stationarity of the augmented cost (18) with respect to \mathbf{v} , while the outer ALM loop updates $\boldsymbol{\lambda}$ to reduce the constraint violation $\|\mathbf{c}\|_2$.

3 Inertia Force Contribution in TL-FEA Formulation

The inertia contribution in Eq. (15) is

$$\delta W_{\text{inertia}} = - \int_{V_r} \rho_r(\mathbf{u}) \delta \mathbf{r}(\mathbf{u}; t)^T \ddot{\mathbf{r}}(\mathbf{u}; t) \, dV_r, \quad (19)$$

where $\rho_r(\mathbf{u})$ is the mass density expressed in the reference configuration and $\mathbf{u} = [u, v, w]^T$ are the material coordinates. Using the TL interpolation $\mathbf{r}(\mathbf{u}; t) = \sum_{i=1}^{n_u} \mathbf{e}_i(t) s_i(\mathbf{u})$, we obtain

$$\delta W_{\text{inertia}} = - \sum_{i=1}^{n_u} \delta \mathbf{e}_i^T \sum_{j=1}^{n_u} m_{ij} \ddot{\mathbf{e}}_j, \quad m_{ij} = \int_{V_r} \rho_r(\mathbf{u}) s_i(\mathbf{u}) s_j(\mathbf{u}) \, dV_r. \quad (20)$$

The coefficients $m_{ij} = m_{ji}$ depend only on reference quantities (ρ_r and the shape functions), hence they are constant and can be precomputed.

It is convenient to introduce the element unknown vector

$$\mathbf{e} = [\mathbf{e}_1^T, \dots, \mathbf{e}_{n_u}^T]^T \in \mathbb{R}^{3n_u}.$$

Equation (20) can then be written as

$$\delta W_{\text{inertia}} = -\delta \mathbf{e}^T \mathbf{M}_e \ddot{\mathbf{e}}, \quad \mathbf{M}_e = [m_{ij} \mathbf{I}_3]_{i,j=1}^{n_u}. \quad (21)$$

After standard FE assembly over all elements, Eq. (21) yields the global inertial virtual work $\delta W_{\text{inertia}} = -\delta \mathbf{q}^T \mathbf{M} \ddot{\mathbf{q}}$, where \mathbf{M} is the global consistent mass matrix. In particular, under the backward-Euler update used to obtain Eq. (17), $\ddot{\mathbf{q}}_{n+1} = \dot{\mathbf{v}}_{n+1} \approx (\mathbf{v}_{n+1} - \mathbf{v}_n)/h$, which leads to the inertial residual contribution $\frac{1}{h} \mathbf{M}(\mathbf{v} - \mathbf{v}_n)$ in Eq. (17).

4 Mass-Distributed Force Field Contribution in TL-FEA Formulation

The force-field component $\delta W_{\text{force-field}}$ in Eq. (15) accounts for mass-distributed loads specified as a force per unit mass. Let $\mathbf{b}(P, t) \in \mathbb{R}^3$ denote such a field (e.g., gravity) evaluated at the current spatial position $P = \mathbf{r}(\mathbf{u}; t)$ of a material point with reference coordinates $\mathbf{u} = [u, v, w]^T$. Its virtual work over a reference volume V_r is

$$\delta W_{\text{force-field}} = \int_{V_r} \rho_r(\mathbf{u}) \delta \mathbf{r}(\mathbf{u}; t)^T \mathbf{b}(\mathbf{r}(\mathbf{u}; t), t) dV_r, \quad (22)$$

where $\rho_r(\mathbf{u})$ is the reference density. Using $\delta \mathbf{r}(\mathbf{u}; t) = \sum_{i=1}^{n_u} \delta \mathbf{e}_i^T s_i(\mathbf{u})$, Eq. (22) becomes

$$\delta W_{\text{force-field}} = \sum_{i=1}^{n_u} \delta \mathbf{e}_i^T \mathbf{f}_i^{\text{ff}}, \quad \mathbf{f}_i^{\text{ff}} := \int_{V_r} \rho_r(\mathbf{u}) s_i(\mathbf{u}) \mathbf{b}(\mathbf{r}(\mathbf{u}; t), t) dV_r \in \mathbb{R}^3. \quad (23)$$

After element assembly, the force-field contribution is collected in \mathbf{f}_{ff} in Eq. (17).

If ρ_r is constant and the field is uniform, $\mathbf{b}(\mathbf{r}(\mathbf{u}; t), t) \equiv \mathbf{b}_0$, then

$$\mathbf{f}_i^{\text{ff}} = \rho_r \mathbf{b}_0 v_i, \quad v_i := \int_{V_r} s_i(\mathbf{u}) dV_r. \quad (24)$$

Note that, although the integration is carried out over V_r , the field must be evaluated at the current position $P = \mathbf{r}(\mathbf{u}; t)$; consequently, \mathbf{b} can vary in time as the body moves through space.

5 Internal Force Contribution in TL-FEA Formulation

The internal force contribution to the equations of motion (EOM) in the Total Lagrangian finite element analysis (TL-FEA) formulation arises from the material's constitutive response to deformation. In the proposed framework, the internal forces are the result of two major components: the hyperelastic material response and the viscous damping effect. The former captures the elastic behavior of the material under finite deformation, while the latter provides numerical stability and models energy dissipation during dynamic simulations.

5.1 Hyperelastic Material Laws

5.1.1 Generic TL internal force expression

The contributions of the internal forces to the EOM for the ANCF beam element and the ANCF 3443 shell element are discussed and derived as follows:

Following the notation used in Eq. 2a, the deformation gradient for the ANCF 3243 element is:

$$\begin{aligned} \mathbf{F} &= \frac{\partial \mathbf{r}}{\partial \mathbf{u}} = \mathbf{N}(t) \cdot \frac{\partial \mathbf{s}}{\partial \mathbf{u}} \\ &= \mathbf{N}(t) \cdot \begin{bmatrix} s_{1,\mathbf{u}} \\ s_{2,\mathbf{u}} \\ s_{3,\mathbf{u}} \\ s_{4,\mathbf{u}} \\ s_{5,\mathbf{u}} \\ s_{6,\mathbf{u}} \\ s_{7,\mathbf{u}} \\ s_{8,\mathbf{u}} \end{bmatrix} = \mathbf{e}_1 s_{1,\mathbf{u}} + \mathbf{e}_2 s_{2,\mathbf{u}} + \dots + \mathbf{e}_8 s_{8,\mathbf{u}} \\ &= \sum_{i=1}^8 \mathbf{e}_i s_{i,\mathbf{u}} \in \mathbb{R}^{3 \times 3}. \end{aligned}$$

Following the notation used earlier, the deformation gradient \mathbf{F} for the 3443 shell element is:

$$\mathbf{F} = \frac{\partial \mathbf{r}}{\partial \mathbf{u}} = \sum_{i=1}^{16} \mathbf{e}_i s_{i,\mathbf{u}} \in \mathbb{R}^{3 \times 3}$$

where each $s_{i,\mathbf{u}} \in \mathbb{R}^{1 \times 3}$.

5.1.2 St Venant–Kirchhoff (SVK) material

The Saint-Venant–Kirchhoff (SVK) material model is a fundamental hyperelastic constitutive model in finite element analysis (FEA), particularly suited to the total Lagrangian formulation, where it employs the Green–Lagrange strain tensor and the second Piola–Kirchhoff stress to capture moderate nonlinear deformations in compressible solids [1]. This model extends classical linear elasticity to finite strains by defining a quadratic strain energy density function $\Psi(\mathbf{E})$ (see (25)), with λ and μ denoting the Lamé constants, making

it computationally straightforward for quasi-static and dynamic simulations of structures undergoing large rotations but limited stretches [2]. Popular in computational mechanics for its simplicity and compatibility with isoparametric elements, the SVK model finds broad use in beam and shell analyses, such as Timoshenko–Ehrenfest beams, biological soft tissues, and multifunctional laminates, although its popularity wanes in extreme compression due to unphysical softening beyond about 58% strain [23]. Despite its limitations in large uniaxial compression, it remains a standard benchmark for validating more advanced hyperelastic models, such as neo-Hookean or Mooney–Rivlin formulations, in FEA software like Abaqus [11].

The strain energy density function is quadratic in \mathbf{E} :

$$\Psi(\mathbf{E}) = \frac{\lambda}{2} (\text{tr}(\mathbf{E}))^2 + \mu \text{tr}(\mathbf{E}^2), \quad (25)$$

where λ and μ are the Lamé constants.

The second Piola–Kirchhoff stress follows from differentiation:

$$\mathbf{S} = \lambda \text{tr}(\mathbf{E}) \mathbf{I} + 2\mu \mathbf{E}. \quad (26)$$

From this, the first Piola–Kirchhoff stress is:

$$\mathbf{P} = \mathbf{FS} = \lambda \text{tr}(\mathbf{E}) \mathbf{F} + 2\mu \mathbf{FE}. \quad (27)$$

Using $\mathbf{E} = \frac{1}{2}(\mathbf{F}^T \mathbf{F} - \mathbf{I})$, this can also be written as:

$$\mathbf{P} = \lambda \left(\frac{1}{2} \text{tr}(\mathbf{F}^T \mathbf{F}) - \frac{3}{2} \right) \mathbf{F} + \mu \mathbf{FF}^T \mathbf{F} - \mu \mathbf{F}. \quad (28)$$

The SVK model is only accurate for small to moderate strains, although it can accommodate arbitrarily large rotations. For large strains, it can give non-physical predictions, such as negative stiffness in compression.

For hyperelastic materials, the first Piola–Kirchhoff stress satisfies $\mathbf{P} = \partial\Psi/\partial\mathbf{F}$; for the SVK model this is consistent with Eqs. (27) and (28).

Using the definition of internal force in the Total Lagrangian setting, the internal force associated with nodal unknown \mathbf{e}_i is, by definition,

$$\mathbf{f}_i^T := \frac{\partial}{\partial \mathbf{e}_i} \int_{V_r} \Psi(\mathbf{E}) dV_r = \int_{V_r} \frac{\partial \Psi(\mathbf{E})}{\partial \mathbf{e}_i} dV_r \quad (29)$$

$$= \int_{V_r} \frac{\partial \Psi(\mathbf{E})}{\partial \mathbf{F}} : \frac{\partial \mathbf{F}}{\partial \mathbf{e}_i} dV_r = \int_{V_r} \mathbf{P} : \frac{\partial \mathbf{F}}{\partial \mathbf{e}_i} dV_r \quad (30)$$

$$= \int_{V_r} (\mathbf{P} \mathbf{h}_i)^T dV_r. \quad (31)$$

which leads to the following result:

$$\mathbf{f}_i = \int_{V_r} \mathbf{P} \mathbf{h}_i dV_r, \quad (32)$$

where \mathbf{P} is the first Piola–Kirchhoff stress tensor and $\mathbf{h}_i := s_{i,\mathbf{u}}^T \in \mathbb{R}^{3 \times 1}$ is the reference-gradient of the shape function $s_i(u, v, w)$. Note that this important

relation holds for *any* hyperelastic material model, not only for the SVK material model. Plugging in the expression of \mathbf{P} for the SVK material model, see (28), we get:

$$\mathbf{f}_i = \int_{V_r} \left[\lambda \left(\frac{1}{2} \text{tr}(\mathbf{F}^T \mathbf{F}) - \frac{3}{2} \right) \mathbf{F} + \mu \mathbf{F} \mathbf{F}^T \mathbf{F} - \mu \mathbf{F} \right] \mathbf{h}_i \, dV_r, \quad (33)$$

and therefore, the expression of the virtual work of the internal force over the element is given by:

$$\delta W_{\text{int}} = \sum_{i=1}^{n_u} \delta \mathbf{e}_i^T \cdot \mathbf{f}_i. \quad (34)$$

Second-order (Newton-type) methods require the consistent linearization of the internal force vector, i.e., the Jacobian (tangent stiffness) $\partial \mathbf{f}_i / \partial \mathbf{e}_j$. For the SVK material model, this Jacobian reads

$$\begin{aligned} \frac{\partial \mathbf{f}_i}{\partial \mathbf{e}_j} = \int_{V_r} & \left[\lambda (\mathbf{F} \mathbf{h}_i) (\mathbf{F} \mathbf{h}_j)^T + \lambda \text{tr}(\mathbf{E}) (\mathbf{h}_j^T \mathbf{h}_i) \mathbf{I} \right. \\ & + \mu (\mathbf{F} \mathbf{h}_j)^T (\mathbf{F} \mathbf{h}_i) \mathbf{I} + \mu (\mathbf{F} \mathbf{h}_j) (\mathbf{F} \mathbf{h}_i)^T \\ & \left. + \mu (\mathbf{h}_j^T \mathbf{h}_i) \mathbf{F} \mathbf{F}^T - \mu (\mathbf{h}_j^T \mathbf{h}_i) \mathbf{I} \right] \, dV_r. \end{aligned} \quad (35)$$

5.1.3 Mooney–Rivlin (MR) material

The Mooney–Rivlin material model is a widely adopted hyperelastic constitutive framework for finite element analysis (FEA) of rubber-like materials, formulated in terms of strain invariants I_1 and I_2 of the right Cauchy–Green tensor to accommodate the near-incompressible behavior of elastomers [14, 16]. In this work, we employ the compressible two-parameter form in (36), which augments the isochoric Mooney–Rivlin response with a volumetric penalty term [1]. The model is effective for moderate to large strains and is widely used for elastomers and soft tissues due to its computational efficiency and compatibility with total Lagrangian formulations [11].

It is expressed directly in terms of the deformation gradient \mathbf{F} and the invariants of the right Cauchy–Green tensor $\mathbf{C} = \mathbf{F}^T \mathbf{F}$. It depends on three material parameters: μ_{10} and μ_{01} (shear response) and k (bulk modulus controlling compressibility). The Mooney–Rivlin model reduces to the neo-Hookean model when $\mu_{01} = 0$, and to a purely incompressible form when $k \rightarrow \infty$ with $J = 1$.

The compressible Mooney–Rivlin strain energy density function is given by

$$\Psi(\mathbf{F}) = \mu_{10} (\bar{I}_1 - 3) + \mu_{01} (\bar{I}_2 - 3) + \frac{k}{2} (J - 1)^2, \quad (36)$$

where

$$\mathbf{C} = \mathbf{F}^T \mathbf{F} \quad (\text{right Cauchy-Green tensor}), \quad (37)$$

$$I_1 = \text{tr}(\mathbf{C}), \quad (38)$$

$$I_2 = \frac{1}{2} [(\text{tr } \mathbf{C})^2 - \text{tr}(\mathbf{C}^2)], \quad (39)$$

$$J = \det \mathbf{F}, \quad (40)$$

$$\bar{I}_1 = J^{-2/3} I_1, \quad (41)$$

$$\bar{I}_2 = J^{-4/3} I_2. \quad (42)$$

The first Piola-Kirchhoff stress can be computed as:

$$\mathbf{P} = \frac{\partial \Psi}{\partial \mathbf{F}} \quad (43)$$

using the chain rule. First, the required derivative identities are:

$$\frac{\partial I_1}{\partial \mathbf{F}} = 2\mathbf{F}, \quad (44)$$

$$\frac{\partial I_2}{\partial \mathbf{F}} = 2(I_1 \mathbf{F} - \mathbf{F} \mathbf{C}), \quad (45)$$

$$\frac{\partial J}{\partial \mathbf{F}} = J \mathbf{F}^{-T}, \quad (46)$$

$$\frac{\partial J^{-m}}{\partial \mathbf{F}} = -m J^{-m} \mathbf{F}^{-T}. \quad (47)$$

Therefore, the computation of the derivatives of the isochoric invariants gives:

$$\begin{aligned} \frac{\partial \bar{I}_1}{\partial \mathbf{F}} &= \frac{\partial (J^{-2/3} I_1)}{\partial \mathbf{F}} = J^{-2/3} \frac{\partial I_1}{\partial \mathbf{F}} + I_1 \frac{\partial J^{-2/3}}{\partial \mathbf{F}} \\ &= J^{-2/3} (2\mathbf{F}) - \frac{2}{3} I_1 J^{-2/3} \mathbf{F}^{-T} \\ &= 2J^{-2/3} \mathbf{F} - \frac{2}{3} J^{-2/3} I_1 \mathbf{F}^{-T}. \end{aligned} \quad (48)$$

Similarly,

$$\begin{aligned} \frac{\partial \bar{I}_2}{\partial \mathbf{F}} &= \frac{\partial (J^{-4/3} I_2)}{\partial \mathbf{F}} \\ &= J^{-4/3} \frac{\partial I_2}{\partial \mathbf{F}} + I_2 \frac{\partial J^{-4/3}}{\partial \mathbf{F}} \\ &= J^{-4/3} [2(I_1 \mathbf{F} - \mathbf{F} \mathbf{C})] - \frac{4}{3} I_2 J^{-4/3} \mathbf{F}^{-T} \\ &= 2J^{-4/3} (I_1 \mathbf{F} - \mathbf{F} \mathbf{C}) - \frac{4}{3} J^{-4/3} I_2 \mathbf{F}^{-T}. \end{aligned} \quad (49)$$

The derivative of the volumetric penalty term is:

$$\frac{\partial}{\partial \mathbf{F}} \left[\frac{k}{2} (J - 1)^2 \right] = k(J - 1) \frac{\partial J}{\partial \mathbf{F}} = k(J - 1) J \mathbf{F}^{-T}. \quad (50)$$

After the final assembly based on the above presented equation:

$$\begin{aligned}
 \mathbf{P} &= \mu_{10} \frac{\partial \bar{I}_1}{\partial \mathbf{F}} + \mu_{01} \frac{\partial \bar{I}_2}{\partial \mathbf{F}} + k(J-1)J\mathbf{F}^{-T} \\
 &= 2\mu_{10}J^{-2/3}\mathbf{F} - \frac{2}{3}\mu_{10}J^{-2/3}I_1\mathbf{F}^{-T} \\
 &\quad + 2\mu_{01}J^{-4/3}(I_1\mathbf{F} - \mathbf{FC}) - \frac{4}{3}\mu_{01}J^{-4/3}I_2\mathbf{F}^{-T} \\
 &\quad + k(J-1)J\mathbf{F}^{-T}.
 \end{aligned} \tag{51}$$

Thus, the first Piola–Kirchhoff stress for the compressible Mooney–Rivlin model is:

$$\begin{aligned}
 \mathbf{P} &= 2\mu_{10}J^{-2/3}(\mathbf{F} - \frac{1}{3}I_1\mathbf{F}^{-T}) \\
 &\quad + 2\mu_{01}J^{-4/3}(I_1\mathbf{F} - \mathbf{FC} - \frac{2}{3}I_2\mathbf{F}^{-T}) \\
 &\quad + k(J-1)J\mathbf{F}^{-T}
 \end{aligned} \tag{52}$$

Using (32) together with (52), the internal force associated with the nodal unknown \mathbf{e}_i admits the decomposition

$$\begin{aligned}
 \mathbf{f}_i &= \mathbf{t}_1 - \mathbf{t}_2 + \mathbf{t}_3 - \mathbf{t}_4 - \mathbf{t}_5 + \mathbf{t}_6, \\
 \mathbf{t}_1 &= 2\mu_{10} \int_{V_r} J^{-2/3} \mathbf{F} \mathbf{h}_i \, dV_r, & \mathbf{t}_4 &= 2\mu_{01} \int_{V_r} J^{-4/3} \mathbf{F} \mathbf{F}^T \mathbf{F} \mathbf{h}_i \, dV_r, \\
 \mathbf{t}_2 &= \frac{2\mu_{10}}{3} \int_{V_r} J^{-2/3} I_1 \mathbf{F}^{-T} \mathbf{h}_i \, dV_r, & \mathbf{t}_5 &= \frac{4\mu_{01}}{3} \int_{V_r} J^{-4/3} I_2 \mathbf{F}^{-T} \mathbf{h}_i \, dV_r, \\
 \mathbf{t}_3 &= 2\mu_{01} \int_{V_r} J^{-4/3} I_1 \mathbf{F} \mathbf{h}_i \, dV_r, & \mathbf{t}_6 &= k \int_{V_r} J(J-1) \mathbf{F}^{-T} \mathbf{h}_i \, dV_r.
 \end{aligned} \tag{53}$$

Second-order (Newton-type) methods require the Jacobian of the internal force, $\mathbf{K}_{ij} := \partial \mathbf{f}_i / \partial \mathbf{e}_j \in \mathbb{R}^{3 \times 3}$. Differentiating (53) yields

$$\begin{aligned}
\frac{\partial \mathbf{f}_i}{\partial \mathbf{e}_j} &= \frac{\partial \mathbf{t}_1}{\partial \mathbf{e}_j} - \frac{\partial \mathbf{t}_2}{\partial \mathbf{e}_j} + \frac{\partial \mathbf{t}_3}{\partial \mathbf{e}_j} - \frac{\partial \mathbf{t}_4}{\partial \mathbf{e}_j} - \frac{\partial \mathbf{t}_5}{\partial \mathbf{e}_j} + \frac{\partial \mathbf{t}_6}{\partial \mathbf{e}_j}, \\
\frac{\partial \mathbf{t}_1}{\partial \mathbf{e}_j} &= 2\mu_{10} \int_{V_r} J^{-2/3} \left[(\mathbf{h}_j^T \mathbf{h}_i) \mathbf{I} - \frac{2}{3} (\mathbf{F} \mathbf{h}_i) (\mathbf{F}^{-T} \mathbf{h}_j)^T \right] dV_r, \\
\frac{\partial \mathbf{t}_2}{\partial \mathbf{e}_j} &= \frac{2\mu_{10}}{3} \int_{V_r} J^{-2/3} \left[(\mathbf{F}^{-T} \mathbf{h}_i) (2\mathbf{F} \mathbf{h}_j)^T \right. \\
&\quad \left. - \frac{2}{3} I_1 (\mathbf{F}^{-T} \mathbf{h}_i) (\mathbf{F}^{-T} \mathbf{h}_j)^T \right. \\
&\quad \left. - I_1 (\mathbf{F}^{-T} \mathbf{h}_j) (\mathbf{F}^{-T} \mathbf{h}_i)^T \right] dV_r, \\
\frac{\partial \mathbf{t}_3}{\partial \mathbf{e}_j} &= 2\mu_{01} \int_{V_r} J^{-4/3} \left[I_1 (\mathbf{h}_j^T \mathbf{h}_i) \mathbf{I} + (\mathbf{F} \mathbf{h}_i) (2\mathbf{F} \mathbf{h}_j)^T \right. \\
&\quad \left. - \frac{4}{3} I_1 (\mathbf{F} \mathbf{h}_i) (\mathbf{F}^{-T} \mathbf{h}_j)^T \right] dV_r, \\
\frac{\partial \mathbf{t}_4}{\partial \mathbf{e}_j} &= 2\mu_{01} \int_{V_r} J^{-4/3} \left[(\mathbf{F} \mathbf{h}_j)^T (\mathbf{F} \mathbf{h}_i) \mathbf{I} + (\mathbf{F} \mathbf{h}_j) (\mathbf{F} \mathbf{h}_i)^T \right. \\
&\quad \left. + (\mathbf{h}_j^T \mathbf{h}_i) \mathbf{F} \mathbf{F}^T - \frac{4}{3} \mathbf{F} \mathbf{F}^T (\mathbf{F} \mathbf{h}_i) (\mathbf{F}^{-T} \mathbf{h}_j)^T \right] dV_r, \\
\frac{\partial \mathbf{t}_5}{\partial \mathbf{e}_j} &= \frac{4\mu_{01}}{3} \int_{V_r} J^{-4/3} \left[(\mathbf{F}^{-T} \mathbf{h}_i) \left(2(\mathbf{F} \mathbf{h}_j)^T (I_1 \mathbf{I} - \mathbf{F} \mathbf{F}^T) \right. \right. \\
&\quad \left. \left. - \frac{4}{3} I_2 (\mathbf{F}^{-T} \mathbf{h}_j)^T \right) - I_2 (\mathbf{F}^{-T} \mathbf{h}_j) (\mathbf{F}^{-T} \mathbf{h}_i)^T \right] dV_r, \\
\frac{\partial \mathbf{t}_6}{\partial \mathbf{e}_j} &= k \int_{V_r} J \left[(2J - 1) (\mathbf{F}^{-T} \mathbf{h}_i) (\mathbf{F}^{-T} \mathbf{h}_j)^T \right. \\
&\quad \left. - (J - 1) (\mathbf{F}^{-T} \mathbf{h}_j) (\mathbf{F}^{-T} \mathbf{h}_i)^T \right] dV_r.
\end{aligned} \tag{54}$$

5.2 Viscous Damping Model in TL-FEA Formulation

5.2.1 Kinematics and Strain-Rate Measure in the Reference Configuration

In the Total Lagrangian setting, all kinematic quantities are expressed with respect to the reference configuration. Let \mathbf{X} denote a material point in the reference configuration and $\mathbf{x}(\mathbf{X}, t)$ its current position at time t . The deformation gradient is

$$\mathbf{F}(\mathbf{X}, t) = \frac{\partial \mathbf{x}}{\partial \mathbf{X}}, \quad J = \det \mathbf{F}. \tag{55}$$

The right Cauchy–Green tensor and Green–Lagrange strain tensor are given by

$$\mathbf{C} = \mathbf{F}^T \mathbf{F}, \quad \mathbf{E} = \frac{1}{2} (\mathbf{C} - \mathbf{I}). \tag{56}$$

The material time derivative of the deformation gradient is

$$\dot{\mathbf{F}} = \frac{\partial \dot{\mathbf{x}}}{\partial \mathbf{X}}, \quad (57)$$

and the corresponding Green–Lagrange strain rate follows from

$$\dot{\mathbf{E}} = \frac{1}{2}(\dot{\mathbf{C}}) = \frac{1}{2}(\dot{\mathbf{F}}^T \mathbf{F} + \mathbf{F}^T \dot{\mathbf{F}}). \quad (58)$$

The tensor $\dot{\mathbf{E}}$ constitutes the basic strain-rate measure used to define viscous damping in the reference configuration.

For the ANCF 3243 beam and 3443 shell elements, the deformation gradient at a given quadrature point can be expressed, following the notation in the previous subsubsections, as

$$\mathbf{F} = \sum_i \mathbf{e}_i \mathbf{s}_{i,\mathbf{u}}, \quad (59)$$

where $\mathbf{e}_i \in \mathbb{R}^3$ denotes the vector of nodal unknowns (position and gradients) and $\mathbf{s}_{i,\mathbf{u}}$ is the row vector of shape-function derivatives with respect to the local coordinates. The time derivative $\dot{\mathbf{F}}$ is then

$$\dot{\mathbf{F}} = \sum_i \dot{\mathbf{e}}_i \mathbf{s}_{i,\mathbf{u}}, \quad (60)$$

and $\dot{\mathbf{E}}$ is obtained from (58). For the T10 element, analogous expressions are obtained by replacing the ANCF basis with the isoparametric T10 shape functions and their reference gradients.

5.2.2 Finite-Strain Kelvin–Voigt Law in the Reference Configuration

The viscous damping model adopted in this work is a finite-strain Kelvin–Voigt law formulated in the reference configuration, where the viscous contribution to the stress depends linearly on the Green–Lagrange strain rate $\dot{\mathbf{E}}$ defined in (58). This type of reference-configuration viscoelastic extension of a hyperelastic backbone is widely used in finite-strain constitutive modeling and finite element formulations, see for example Simo [19], Reese and Govindjee [15], Holzapfel [7], Holzapfel and Simo [8], and Treutenaere et al. [20]. The total second Piola–Kirchhoff stress \mathbf{S} is decomposed into an elastic and a viscous contribution,

$$\mathbf{S} = \mathbf{S}^{\text{el}} + \mathbf{S}^{\text{vis}}, \quad (61)$$

where \mathbf{S}^{el} is provided by the chosen hyperelastic backbone (SVK or Mooney–Rivlin), and \mathbf{S}^{vis} is a linear function of $\dot{\mathbf{E}}$ of Kelvin–Voigt type.

In analogy with the small-strain isotropic Kelvin–Voigt model, the viscous second Piola–Kirchhoff stress is chosen as

$$\mathbf{S}^{\text{vis}} = 2\eta \dot{\mathbf{E}} + \lambda_v \text{tr}(\dot{\mathbf{E}}) \mathbf{I}, \quad (62)$$

where $\eta \geq 0$ and $\lambda_v \geq 0$ are viscosity-like parameters that play a role analogous to the shear and bulk Lamé constants in the elastic law. The total first Piola–Kirchhoff stress then becomes

$$\mathbf{P} = \mathbf{F} \mathbf{S} = \mathbf{F} \mathbf{S}^{\text{el}} + \mathbf{F} \mathbf{S}^{\text{vis}} = \mathbf{P}^{\text{el}} + \mathbf{P}^{\text{vis}}, \quad (63)$$

with

$$\mathbf{P}^{\text{el}} = \mathbf{F} \mathbf{S}^{\text{el}}, \quad \mathbf{P}^{\text{vis}} = \mathbf{F} \mathbf{S}^{\text{vis}}. \quad (64)$$

This formulation is compatible with both SVK and Mooney–Rivlin hyperelastic models, since only the elastic part \mathbf{S}^{el} changes when switching the constitutive backbone, while the viscous Kelvin–Voigt contribution (62) retains the same structure [19, 15, 7].

5.2.3 Dissipation and Thermodynamic Consistency

The viscous part of the stress should dissipate, rather than create, mechanical energy. In the reference configuration, the power of internal forces per unit reference volume associated with the viscous stress is

$$\dot{W}_{\text{diss}} = \mathbf{S}^{\text{vis}} : \dot{\mathbf{E}}. \quad (65)$$

Using the Kelvin–Voigt law (62),

$$\begin{aligned} \dot{W}_{\text{diss}} &= (2\eta \dot{\mathbf{E}} + \lambda_v \text{tr}(\dot{\mathbf{E}}) \mathbf{I}) : \dot{\mathbf{E}} \\ &= 2\eta \dot{\mathbf{E}} : \dot{\mathbf{E}} + \lambda_v \text{tr}(\dot{\mathbf{E}}) (\mathbf{I} : \dot{\mathbf{E}}) \\ &= 2\eta \dot{\mathbf{E}} : \dot{\mathbf{E}} + \lambda_v [\text{tr}(\dot{\mathbf{E}})]^2. \end{aligned} \quad (66)$$

Both terms on the right-hand side are quadratic forms in $\dot{\mathbf{E}}$. For $\eta \geq 0$ and $\lambda_v \geq 0$ one obtains

$$\dot{W}_{\text{diss}} \geq 0 \quad (67)$$

for all admissible strain rates, so that the viscous model is thermodynamically consistent in the sense that it cannot generate mechanical energy. This type of quadratic dissipation potential and non-negativity requirement is standard in finite-strain viscoelastic theories [19, 15, 7, 8, 20]. In particular, \dot{W}_{diss} vanishes if and only if $\dot{\mathbf{E}} = \mathbf{0}$, corresponding to a configuration with no strain evolution.

5.2.4 Element-Level Formulation with Viscous Damping

The derivation of the internal nodal forces for hyperelastic materials in the Total Lagrangian formulation leads to

$$\mathbf{f}_i = \int_{V_r} \mathbf{P} \mathbf{h}_i \, dV_r, \quad (68)$$

where V_r is the element volume in the reference configuration, \mathbf{P} is the first Piola–Kirchhoff stress, and \mathbf{h}_i denotes the Jacobian (with respect to \mathbf{X}) of the

shape function corresponding to nodal unknown \mathbf{e}_i . This expression holds for any hyperelastic constitutive model, as discussed earlier.

When the viscous contribution (63) is included, the internal force naturally splits into an elastic part and a viscous part,

$$\mathbf{f}_i = \mathbf{f}_i^{\text{el}} + \mathbf{f}_i^{\text{vis}}, \quad (69)$$

with

$$\mathbf{f}_i^{\text{el}} = \int_{V_r} \mathbf{P}^{\text{el}} \mathbf{h}_i \, dV_r, \quad \mathbf{f}_i^{\text{vis}} = \int_{V_r} \mathbf{P}^{\text{vis}} \mathbf{h}_i \, dV_r. \quad (70)$$

Using $\mathbf{P}^{\text{vis}} = \mathbf{F} \mathbf{S}^{\text{vis}}$ and (62), the viscous force contribution at a quadrature point is computed as follows:

1. Assemble \mathbf{F} from the current nodal unknowns (ANCF gradients or T10 displacements) and shape-function gradients.
2. Assemble $\dot{\mathbf{F}}$ from the current nodal velocities and the same shape-function gradients.
3. Compute $\dot{\mathbf{E}}$ using (58).
4. Evaluate \mathbf{S}^{vis} by (62).
5. Form $\mathbf{P}^{\text{vis}} = \mathbf{F} \mathbf{S}^{\text{vis}}$.
6. Accumulate the contribution $\mathbf{P}^{\text{vis}} \mathbf{h}_i$ into $\mathbf{f}_i^{\text{vis}}$ at the quadrature point, multiply by the geometric Jacobian and quadrature weight, and sum over all quadrature points.

The total internal force vector for the element is the sum of the elastic and viscous contributions. This procedure is identical for the ANCF 3243 beam, ANCF 3443 shell, and T10 solid elements, differing only in the specific definitions of the shape functions and their reference gradients.

The corresponding contribution to the element tangent matrix (if an implicit time integrator is employed) can be obtained by linearizing $\mathbf{f}_i^{\text{vis}}$ with respect to the nodal velocities and displacements. In the present work, the viscous term is primarily used to regularize the explicit dynamics and to introduce physically motivated damping; therefore, an explicit evaluation of $\mathbf{f}_i^{\text{vis}}$ is sufficient.

6 External Force Contribution in TL-FEA Formulation

In the proposed TL-FEA formulation, the external force contribution to the equations of motion (EOM) in the majority of cases falls under two categories: a pointwise external force load, which is trivial, and friction and contact forces formulated as externally applied forces, which involve a friction and contact force model. In this section, we discuss the handling of both types of external forces.

6.1 Pointwise External Force Loads

When a pointwise external force load is applied to an element, it shall be distributed to the nodes of the element according to the shape functions. The external force contribution for this component is relatively trivial.

The pointwise applied-load component of $\delta W_{\text{applied}}$ in Eq. (15) accounts for forces concentrated at material points. Consider an external force $\mathbf{f}_P(t) \in \mathbb{R}^3$ applied at a point P of reference coordinates $\mathbf{u}_P = [u, v, w]^T$. Its virtual work contribution is

$$\delta W_{\text{applied}}^P = \delta \mathbf{r}(\mathbf{u}_P; t)^T \mathbf{f}_P(t). \quad (71)$$

Using the TL interpolation $\delta \mathbf{r}(\mathbf{u}; t) = \sum_{i=1}^{n_u} \delta \mathbf{e}_i^T s_i(\mathbf{u})$, Eq. (71) becomes

$$\delta W_{\text{applied}}^P = \sum_{i=1}^{n_u} \delta \mathbf{e}_i^T \mathbf{f}_{iP}, \quad \mathbf{f}_{iP} := s_i(\mathbf{u}_P) \mathbf{f}_P(t) \in \mathbb{R}^3. \quad (72)$$

Therefore, a pointwise force is distributed to the element nodal unknowns according to the shape functions evaluated at \mathbf{u}_P . After assembly over all pointwise loads and elements, these contributions are collected in the external force vector \mathbf{f}_{ext} in Eq. (17).

6.2 Friction and Contact Handling in TL-FEA Formulation

In the proposed TL-FEA formulation, we handle friction and contact using a penalty-based contact law with damping and history-dependent tangential friction. Note that the model is piecewise (compressive-only normal response via $\max(0, \cdot)$ and stick-slip branching) and is therefore nonsmooth at regime transitions; if a differentiable operator is required, one may replace $\max(0, x)$ with $\frac{1}{2}(x + \sqrt{x^2 + \varepsilon^2})$ and adopt a regularized Coulomb law. At each active contact, forces are evaluated from the penetration depth and relative velocity at the contact point, and assembled into the external force vector \mathbf{f}_{ext} in Eq. (17).

We adopt a damped Hertz-type model for the normal response and a Mindlin history-dependent model for tangential friction.

6.2.1 Contact kinematics and activation

Consider two bodies A and B in contact at point \mathbf{x}_c . Let \mathbf{n} be the unit normal pointing from B to A, and let δ denote the penetration depth (contact active when $\delta > 0$). Define the relative velocity at the contact point as $\mathbf{v}_{\text{rel}} = \mathbf{v}_A(\mathbf{x}_c) - \mathbf{v}_B(\mathbf{x}_c)$, with normal and tangential components

$$v_n = \mathbf{v}_{\text{rel}} \cdot \mathbf{n}, \quad \mathbf{v}_t = \mathbf{v}_{\text{rel}} - v_n \mathbf{n}. \quad (73)$$

The contact traction is applied in action-reaction form: $\mathbf{F}_{c,A} = \mathbf{F}_n + \mathbf{F}_t$ and $\mathbf{F}_{c,B} = -\mathbf{F}_{c,A}$. When $\delta \leq 0$, we set $\mathbf{F}_n = \mathbf{F}_t = \mathbf{0}$ and reset the tangential history variable (Section 6.2.3).

6.2.2 Damped Hertz-type normal law

We use an effective elastic modulus [9]

$$\frac{1}{E_{\text{eff}}} = \frac{1 - \nu_A^2}{E_A} + \frac{1 - \nu_B^2}{E_B}. \quad (74)$$

To accommodate both sphere-like and patch-based contacts, we introduce an effective contact radius a . For smooth spheres, $a = \sqrt{R_{\text{eff}}\delta}$ with $R_{\text{eff}}^{-1} = R_A^{-1} + R_B^{-1}$; for a triangle/patch contact of area A_{patch} , we use the equivalent disk radius $a = \sqrt{A_{\text{patch}}/\pi}$. With the stiffness scale $S_n = 2E_{\text{eff}}a$ and coefficient $k_n = \frac{2}{3}S_n = \frac{4}{3}E_{\text{eff}}a$, the elastic contribution is $k_n\delta$, which recovers the classical Hertz scaling $F_n \propto \delta^{3/2}$ when $a = \sqrt{R_{\text{eff}}\delta}$.

To model dissipation, we use a restitution-based damping parameter [3, 21]

$$\beta = \frac{\ln(e)}{\sqrt{\ln(e)^2 + \pi^2}}, \quad e \in (0, 1], \quad (75)$$

and define the (nonnegative) normal damping coefficient

$$\gamma_n = -2\sqrt{\frac{5}{6}}\beta\sqrt{S_n m_{\text{eff}}}. \quad (76)$$

Here m_{eff} is an effective mass at the contact; for scalar masses it reduces to $m_{\text{eff}} = (m_A^{-1} + m_B^{-1})^{-1}$. The normal contact force is

$$\mathbf{F}_n = F_n \mathbf{n}, \quad F_n = \max(0, k_n\delta - \gamma_n v_n), \quad (77)$$

which enforces a compressive-only response and yields a repulsive damping contribution on approach ($v_n < 0$).

6.2.3 Mindlin history-dependent tangential friction

We model tangential traction using a Mindlin-type incremental stiffness with a history (stiction) variable [12, 13, 4]. Let δ_t denote the stored tangential spring displacement for each contact. At each step, we update and re-project it onto the current tangent plane,

$$\delta_t \leftarrow (\mathbf{I} - \mathbf{n}\mathbf{n}^T)(\delta_t + \Delta t \mathbf{v}_t). \quad (78)$$

We define the effective shear modulus as $G_i = E_i/(2(1 + \nu_i))$ and

$$\frac{1}{G_{\text{eff}}} = \frac{2 - \nu_A}{G_A} + \frac{2 - \nu_B}{G_B}. \quad (79)$$

The tangential stiffness and damping are

$$k_t = 8G_{\text{eff}}a, \quad \gamma_t = -2\sqrt{\frac{5}{6}}\beta\sqrt{m_{\text{eff}}k_t}, \quad (80)$$

and the trial tangential force is

$$\mathbf{F}_t^{\text{trial}} = -k_t \boldsymbol{\delta}_t - \gamma_t \mathbf{v}_t. \quad (81)$$

With a Coulomb limit $F_{\max} = \mu \|\mathbf{F}_n\|$, we set

$$\mathbf{F}_t = \begin{cases} \mathbf{F}_t^{\text{trial}}, & \|\mathbf{F}_t^{\text{trial}}\| \leq F_{\max} \quad (\text{stick}), \\ \frac{F_{\max}}{\|\mathbf{F}_t^{\text{trial}}\|} \mathbf{F}_t^{\text{trial}}, & \|\mathbf{F}_t^{\text{trial}}\| > F_{\max} \quad (\text{slip}). \end{cases} \quad (82)$$

In the slip regime, we rewind the history variable to keep $\mathbf{F}_t = -k_t \boldsymbol{\delta}_t - \gamma_t \mathbf{v}_t$ consistent with the capped force:

$$\boldsymbol{\delta}_t \leftarrow -\frac{\mathbf{F}_t + \gamma_t \mathbf{v}_t}{k_t}. \quad (83)$$

This update reduces chatter by ensuring that the next step starts from the Coulomb boundary rather than from an over-extended tangential spring.

Finally, once \mathbf{F}_n and \mathbf{F}_t are evaluated at the contact point, they are treated as instantaneous external forces applied to the corresponding element(s) in action–reaction form. The resulting nodal load distribution follows the same procedure as for pointwise external force loads in Section 6.1.

7 Kinematic Constraint Handling in TL-FEA Formulation

Following the taxonomy proposed in [10], we introduce the following four basic geometric constraints: dot-product 1 (DP1), dot-product 2 (DP2), distance (DIST), and pin (PIN). The DP1 constraint brings into play four points: points P and Q that belong to elements E and F on body b, respectively, and points R and T that belong to body c's elements G and H, respectively. This constraint requires that the dot product between the vector from P to Q and the vector from R to T is equal to a user-prescribed function of time, $f(t)$, where $f : \mathbb{R}_+ \rightarrow \mathbb{R}$. In many cases, this function is constant and zero for all time t , in which case the constraint becomes a perpendicularity requirement. Using the TL-FEA framework proposed, DP1 assumes the following form:

$$[\mathbf{N}_F^b(t) \mathbf{s}_F^b(Q) - \mathbf{N}_E^b(t) \mathbf{s}_E^b(P)]^T [\mathbf{N}_H^c(t) \mathbf{s}_H^c(T) - \mathbf{N}_G^c(t) \mathbf{s}_G^c(R)] - f(t) = 0. \quad (84)$$

Similar expressions can be written for the other three basic geometric constraints. DP2 is similar to DP1, but it places the point R on the body that points P and Q belong to. The DIST constraint states that the distance between two points (which can belong to the same element, or same body, or different bodies) should assume a strictly positive, user-prescribed value, possibly time-varying. The PIN constraint states that two points (which can belong to the same element, or same body, or different bodies) coincide at all times. Based on this taxonomy, one can build typical engineering joints such as spherical (one PIN constraint), universal (one PIN & one DP1), cylindrical (two DP1 and two DP2), revolute (one PIN and two DP1), translational (three DP1 and two DP2), etc.

References

1. Bonet, J., Wood, R.D.: *Nonlinear Continuum Mechanics for Finite Element Analysis*, 2nd edn. Cambridge University Press, Cambridge, UK (2008). DOI 10.1017/CBO9780511755446
2. Bonet, J., et al.: Limitations of the st. venant–kirchhoff material model in large strain applications. *International Journal of Solids and Structures* **248**, 111618 (2022). DOI 10.1016/j.ijsolstr.2022.111618. URL <https://www.sciencedirect.com/science/article/abs/pii/S0020746222001810>
3. Brilliantov, N.V., Pöschel, T.: Rolling friction of a viscous sphere on a hard plane. *Europhysics Letters (EPL)* **42**(5), 511–516 (1998). DOI 10.1209/epl/i1998-00281-7. URL <https://doi.org/10.1209%2Fep1%2Fi1998-00281-7>
4. Fleischmann, J., Serban, R., Negruț, D., Jayakumar, P.: On the importance of displacement history in soft-body contact models. *Journal of Computational and Nonlinear Dynamics* **11**(4), 044502 (2016)
5. Gerstmayr, J., Shabana, A.A.: Efficient integration of the elastic forces and thin three-dimensional beam elements in the absolute nodal coordinate formulation. In: *Proceeding of Multibody Dynamics ECCOMAS Thematic Conference*. Madrid, Spain (2005)
6. Geuzaine, C., Remacle, J.F.: Gmsh: A 3-D finite element mesh generator with built-in pre- and post-processing facilities. *International Journal for Numerical Methods in Engineering* **79**(11), 1309–1331 (2009). DOI 10.1002/nme.2579. URL <https://doi.org/10.1002/nme.2579>
7. Holzapfel, G.A.: On large strain viscoelasticity: Continuum formulation and finite element applications to elastomeric structures. *International Journal for Numerical Methods in Engineering* **39**(22), 3903–3926 (1996). DOI 10.1002/(SICI)1097-0207(19961130)39:22<3903::AID-NME34>3.0.CO;2-C
8. Holzapfel, G.A., Simo, J.C.: A new viscoelastic constitutive model for continuous media at finite thermomechanical changes. *International Journal of Solids and Structures* **33**(20–22), 3019–3034 (1996). DOI 10.1016/0020-7683(95)00263-4
9. Johnson, K.L.: *Contact Mechanics*. Cambridge University Press (1987)
10. Kissel, A., Taves, J., Negruț, D.: Constrained multibody kinematics and dynamics in absolute coordinates: A discussion of three approaches to representing rigid body rotation. *Journal of Computational and Nonlinear Dynamics* **17**(10), 101008 (2022). DOI 10.1115/1.4055140. URL <https://doi.org/10.1115/1.4055140.101008>
11. Luo, Y., Peng, B.: Benchmark problems of hyper-elasticity analysis in evaluation of fem. *Applied Sciences* **10**(4), 1240 (2020). DOI 10.3390/app10041240
12. Mindlin, R.: Compliance of elastic bodies in contact. *J. of Appl. Mech.* **16** (1949)
13. Mindlin, R., Deresiewicz, H.: Elastic spheres in contact under varying oblique forces. *Journal of Applied Mechanics* **20**, 327–344 (1953)
14. Mooney, M.: A theory of large elastic deformation. *Journal of Applied Physics* **11**(9), 582–592 (1940). DOI 10.1063/1.1712836
15. Reese, S., Govindjee, S.: A theory of finite viscoelasticity and numerical aspects. *International Journal of Solids and Structures* **35**(26–27), 3455–3482 (1998). DOI 10.1016/S0020-7683(97)00217-5
16. Rivlin, R.S.: Large elastic deformations of isotropic materials. I. Fundamental concepts. *Philosophical Transactions of the Royal Society of London. Series A, Mathematical and Physical Sciences* **240**(822), 459–490 (1948). DOI 10.1098/rsta.1948.0002
17. Shabana, A., Yakoub, R.: Three dimensional absolute nodal coordinate formulation for beam elements: Theory. *ASME J. Mech. Design* **123**, 606–613 (2001)
18. Si, H.: TetGen, a delaunay-based quality tetrahedral mesh generator. *ACM Transactions on Mathematical Software* **41**(2) (2015). DOI 10.1145/2629697. URL <https://doi.org/10.1145/2629697>
19. Simo, J.C.: On a fully three-dimensional finite-strain viscoelastic damage model: Formulation and computational aspects. *Computer Methods in Applied Mechanics and Engineering* **60**(2), 153–173 (1987). DOI 10.1016/0045-7825(87)90107-1
20. Treutenaere, S., Lauro, F., Bennani, B., Matsumoto, T., Mottola, E.: Finite strain formulation of viscoelastic damage model for simulation of fabric reinforced polymers under dynamic loading. In: *EPJ Web of Conferences*, vol. 94, p. 04011 (2015). DOI 10.1051/epjconf/20159404011

21. Tsuji, Y., Tanaka, T., Ishida, T.: Lagrangian numerical simulation of plug flow of cohesionless particles in a horizontal pipe. *Powder Technology* **71**(3), 239–250 (1992)
22. Zienkiewicz, O., Taylor, R.: *The Finite Element Method for Solid and Structural Mechanics*, 6 edn. Butterworth-Heinemann (2005)
23. Źur, K., Firouzi, N., Rabczuk, T., Zhuang, X.: Large deformation of hyperelastic modified timoshenko–ehrenfest beams under different types of loads. *Computer Methods in Applied Mechanics and Engineering* **416**, 116368 (2023). DOI 10.1016/j.cma.2023.116368. URL <https://www.sciencedirect.com/science/article/abs/pii/S0045782523004929>